Laboratory experiments for inter-comparison of three volume scattering meters to measure angular scattering properties of hydrosols

T. Harmel,[1,2,*] M. Hieronymi,[3] W. Slade,[4] R. Röttgers,[3] F. Roullier[1] and M. Chami[1,5]

[1]*Sorbonne Universités, UPMC Univ Paris 06, INSU-CNRS, Laboratoire d'Océanographie de Villefranche, 181 Chemin du Lazaret, 06230 Villefranche sur Mer, France*
[2]*IRSTEA, UR MALY, ONEMA/IRSTEA Rivers Hydroecology Research Unit, Lyon-Villeurbanne, France*
[3]*Helmholtz-Zentrum Geesthacht, Center for Materials and Coastal Research, Institute for Coastal Research, Max-Planck-Str. 1, 21502 Geesthacht, Germany*
[4]*Sequoia Scientific, Inc., 2700 Richards Road, Suite 107, Bellevue, Washington 98005, USA*
[5]*Institut Universitaire de France, 1, rue Descartes, 75231 Paris Cedex 05, France*
[*]*harmel@obs-vlfr.fr*

Abstract: Measurements of the volume scattering function (VSF) of hydrosols is of primary importance to investigate the interaction of light with hydrosols and to further interpret in situ and remote sensing data of ocean color. In this paper, a laboratory inter-comparison experiment of three recently developed VSF meters that are able to measure the scattered light for a wide range of scattering angle at 515 nm wavelength is performed using phytoplankton cultures and mineral-like hydrosols. A rigorous measurement protocol was employed to ensure good quality data. In particular, the protocol enabled removing the influence of bacteria on the hydrosols within the sample. The differences in the VSF measurements between the instruments vary from 10 to 25% depending on the composition of the hydrosols. The analysis of the angular features of the VSF revealed a sharp increase of the VSF beyond the scattering angle of 150° for some phytoplankton species. Such behavior is observed for two of the three VSF meters, thus suggesting that it is not due to instrumental artifacts but more likely to phytoplankton optical properties themselves. Moreover, comparisons with currently used theoretical phase functions show that the models are not able to reproduce satisfactorily the directional patterns in the backscattering region. This study suggests that a better modelling of the VSF shape of phytoplankton at high scattering angles is required to correctly represent the angular shape of the VSF in the backscattering hemisphere. Tabulated values of the measured phase functions are provided for scattering angles from 0.1 to 175°.

OCIS codes: (010.4450) Oceanic optics; (120.5820) Scattering measurements.

References and links

1. T. Dickey, M. Lewis, and G. Chang, "Optical oceanography: recent advances and future directions using global remote sensing and in situ observations," Rev. Geophys. **44**(1), RG1001 (2006), doi:10.1029/2003RG000148.
2. M. J. Behrenfeld, R. T. O'Malley, D. A. Siegel, C. R. McClain, J. L. Sarmiento, G. C. Feldman, A. J. Milligan, P. G. Falkowski, R. M. Letelier, and E. S. Boss, "Climate-driven trends in contemporary ocean productivity," Nature **444**(7120), 752–755 (2006).
3. C. R. McClain, "A decade of satellite ocean color observations," Annu. Rev. Mar. Sci. **1**(1), 19–42 (2009).
4. J. Dauchet, S. Blanco, J.-F. Cornet, and R. Fournier, "Calculation of the radiative properties of photosynthetic microorganisms," J. Quant. Spectrosc. Radiat. Transf. **161**, 60–84 (2015).
5. X. Zhang, M. Twardowski, and M. Lewis, "Retrieving composition and sizes of oceanic particle subpopulations from the volume scattering function," Appl. Opt. **50**(9), 1240–1259 (2011).

#251344 Received 2 Oct 2015; revised 4 Dec 2015; accepted 4 Dec 2015; published 15 Dec 2015

6. M. Babin, D. Stramski, R. A. Reynolds, V. M. Wright, and E. Leymarie, "Determination of the volume scattering function of aqueous particle suspensions with a laboratory multi-angle light scattering instrument," Appl. Opt. **51**(17), 3853–3873 (2012).
7. M. E. Lee and M. R. Lewis, "A new method for the measurement of the optical volume scattering function in the upper ocean," J. Atmos. Ocean. Technol. **20**(4), 563–571 (2003).
8. J. Sullivan, M. Twardowski, J. Ronald, V. Zaneveld, and C. Moore, "Measuring optical backscattering in water," in *Light Scattering Reviews 7*, Springer Praxis Books (Springer Berlin Heidelberg, 2013), pp. 189–224.
9. T. J. Petzold, *Volume Scattering Functions for Selected Ocean Waters* (DTIC Document, 1972).
10. G. Kullenberg, "Scattering of light by Sargasso Sea water," Deep-Sea Res. **15**, 425–432 (1968).
11. H. Tan, T. Oishi, A. Tanaka, and R. Doerffer, "Accurate estimation of the backscattering coefficient by light scattering at two backward angles," Appl. Opt. **54**(25), 7718–7733 (2015).
12. W. H. Slade, Y. C. Agrawal, and O. A. Mikkelsen, "Comparison of measured and theoretical scattering and polarization properties of narrow size range irregular sediment particles," in *Oceans* (2013), pp. 23–27.
13. J. K. Lotsberg, E. Marken, J. J. Stamnes, S. R. Erga, K. Aursland, and C. Olseng, "Laboratory measurements of light scattering from marine particles," Limnol. Oceanogr. Methods **5**, 34–40 (2007).
14. M. E. Zugger, A. Messmer, T. J. Kane, J. Prentice, B. Concannon, A. Laux, and L. Mullen, "Optical scattering properties of phytoplankton: Measurements and comparison of various species at scattering angles between 1° and 170°," Limnol. Oceanogr. **53**(1), 381–386 (2008).
15. J. M. Sullivan and M. S. Twardowski, "Angular shape of the oceanic particulate volume scattering function in the backward direction," Appl. Opt. **48**(35), 6811–6819 (2009).
16. B. Shao, J. S. Jaffe, M. Chachisvilis, and S. C. Esener, "Angular resolved light scattering for discriminating among marine picoplankton: modeling and experimental measurements," Opt. Express **14**(25), 12473–12484 (2006).
17. M. Chami, A. Thirouard, and T. Harmel, "POLVSM (Polarized Volume Scattering Meter) instrument: an innovative device to measure the directional and polarized scattering properties of hydrosols," Opt. Express **22**(21), 26403–26428 (2014).
18. Ø. Svensen, J. J. Stamnes, M. Kildemo, L. M. S. Aas, S. R. Erga, and Ø. Frette, "Mueller matrix measurements of algae with different shape and size distributions," Appl. Opt. **50**(26), 5149–5157 (2011).
19. H. Tan, R. Doerffer, T. Oishi, and A. Tanaka, "A new approach to measure the volume scattering function," Opt. Express **21**(16), 18697–18711 (2013).
20. H. Tan, "A new method for the simultaneous determination of volume scattering functions," PhD dissertation, Universität Hamburg (2014).
21. Y. C. Agrawal, "The optical volume scattering function: Temporal and vertical variability in the water column off the New Jersey coast," Limnol. Oceanogr. **50**(6), 1787–1794 (2005).
22. W. H. Slade and E. S. Boss, "Calibrated near-forward volume scattering function obtained from the LISST particle sizer," Opt. Express **14**(8), 3602–3615 (2006).
23. R. Röttgers, C. Häse, and R. Doerffer, "Determination of the particulate absorption of microalgae using a point-source integrating-cavity absorption meter: verification with a photometric technique, improvements for pigment bleaching, and correction for chlorophyll fluorescence," Limnol. Oceanogr. Methods **5**, 1–12 (2007).
24. R. Röttgers, D. McKee, and C. Utschig, "Temperature and salinity correction coefficients for light absorption by water in the visible to infrared spectral region," Opt. Express **22**(21), 25093–25108 (2014).
25. X. Zhang and L. Hu, "Scattering by pure seawater at high salinity," Opt. Express **17**(15), 12685–12691 (2009).
26. R. Röttgers and R. Doerffer, "Measurements of optical absorption by chromophoric dissolved organic matter using a point-source integrating-cavity absorption meter," Limnol. Oceanogr. Methods **5**(5), 126–135 (2007).
27. I. Shihira and R. W. Krauss, *Chlorella: Physiology and Taxonomy of Forty-One Isolates* (University of Maryland, 1965).
28. B. E. F. Reimann and J. C. Lewin, "The diatom genus Cylindrotheca Rabenhorst," J. R. Microsc. Soc. **83**(3), 283–296 (1964).
29. E. C. Teodoresco, "Organisation et développement du Dunaliella. nouveau genre de Volvocacée-Polyblépharidée.," Beihefte zum Bot. Cent. **18**, 215–232 (1905).
30. N. Daugbjerg, G. Hansen, J. Larsen, and Ø. Moestrup, "Phylogeny of some of the major genera of dinoflagellates based on ultrastructure and partial LSU rDNA sequence data, including the erection of three new genera of unarmoured dinoflagellates," Phycologia **39**(4), 302–317 (2000).
31. P. T. Cleve, "Examination of diatoms found on the surface of the sea of Java," Bih. Kongl. Sven. Vetensk.-Akad. Handl. **1**, 1–13 (1873).
32. G. Mie, "Beitrage zur Optik truber Medien, speziell kolloidaler Metallosungen," Ann. Phys. **330**(3), 377–445 (1908).
33. D. Stramski, E. Boss, D. Bogucki, and K. J. Voss, "The role of seawater constituents in light backscattering in the ocean," Prog. Oceanogr. **61**(1), 27–56 (2004).
34. C. D. Mobley, L. K. Sundman, and E. Boss, "Phase function effects on oceanic light fields," Appl. Opt. **41**(6), 1035–1050 (2002).
35. A. L. Whitmire, W. S. Pegau, L. Karp-Boss, E. Boss, and T. J. Cowles, "Spectral backscattering properties of marine phytoplankton cultures," Opt. Express **18**(14), 15073–15093 (2010).

#251344 Received 2 Oct 2015; revised 4 Dec 2015; accepted 4 Dec 2015; published 15 Dec 2015

36. R. D. Vaillancourt, C. W. Brown, R. R. L. Guillard, and W. M. Balch, "Light backscattering properties of marine phytoplankton: relationships to cell size, chemical composition and taxonomy," J. Plankton Res. **26**(2), 191–212 (2004).
37. A. L. Whitmire, E. Boss, T. J. Cowles, and W. S. Pegau, "Spectral variability of the particulate backscattering ratio," Opt. Express **15**(11), 7019–7031 (2007).
38. G. R. Fournier and J. L. Forand, "Analytic phase function for ocean water," in *Ocean Optics XII* (International Society for Optics and Photonics, 1994), pp. 194–201.
39. H. Volten, J. F. Haan, J. W. Hovenier, R. Schreurs, W. Vassen, A. G. Dekker, H. J. Hoogenboom, F. Charlton, and R. Wouts, "Laboratory measurements of angular distributions of light scattered by phytoplankton and silt," Limnol. Oceanogr. **43**(6), 1180–1197 (1998).
40. X. Zhang, E. Boss, and D. J. Gray, "Significance of scattering by oceanic particles at angles around 120 degree," Opt. Express **22**(25), 31329–31336 (2014).
41. D. Watson, N. Hagen, J. Diver, P. Marchand, and M. Chachisvilis, "Elastic Light Scattering from Single Cells: Orientational Dynamics in Optical Trap," Biophys. J. **87**(2), 1298–1306 (2004).
42. K. J. Voss and E. S. Fry, "Measurement Of The Mueller Matrix For Ocean Water," Appl. Opt. **23**(23), 4427–4439 (1984).
43. M. Chami, D. McKee, E. Leymarie, and G. Khomenko, "Influence of the angular shape of the volume-scattering function and multiple scattering on remote sensing reflectance," Appl. Opt. **45**(36), 9210–9220 (2006).
44. J. K. Lotsberg and J. J. Stamnes, "Impact of particulate oceanic composition on the radiance and polarization of underwater and backscattered light," Opt. Express **18**(10), 10432–10445 (2010).
45. J. C. Kitchen and J. R. V. Zaneveld, "A three layered sphere model of the optical properties of phytoplankton," Limnol. Oceanogr. **37**(8), 1680–1690 (1992).
46. T. Oishi, "Significant relationship between the backward scattering coefficient of sea water and the scatterance at 120 °," Appl. Opt. **29**(31), 4658–4665 (1990).
47. E. Boss and W. S. Pegau, "Relationship of light scattering at an angle in the backward direction to the backscattering coefficient," Appl. Opt. **40**(30), 5503–5507 (2001).
48. J.-F. Berthon, E. Shybanov, M. E.-G. Lee, and G. Zibordi, "Measurements and modeling of the volume scattering function in the coastal northern Adriatic Sea," Appl. Opt. **46**(22), 5189–5203 (2007).
49. M. Chami, E. Marken, J. J. Stamnes, G. Khomenko, and G. Korotaev, "Variability of the relationship between the particulate backscattering coefficient and the volume scattering function measured at fixed angles," J. Geophys. Res. **111**(C5), C05013 (2006).
50. H. Claustre, A. Morel, S. B. Hooker, M. Babin, D. Antoine, K. Oubelkheir, A. Bricaud, K. Leblanc, B. Quéguiner, and S. Maritorena, "Is desert dust making oligotrophic waters greener?" Geophys. Res. Lett. **29**(10), 107–111 (2002).
51. G. Volpe, V. F. Banzon, R. H. Evans, R. Santoleri, A. J. Mariano, and R. Sciarra, "Satellite observations of the impact of dust in a low-nutrient, low-chlorophyll region: Fertilization or artifact?" Global Biogeochem. Cycles **23**(3), GB3007 (2009).

1. Introduction

Propagation of light within a given medium is governed by two essential optical properties: absorption and scattering. The characterization of these properties for living and non-living particles in aquatic environment (ocean or lakes) is a prerequisite to understand the temporal and spatial variability of light within the water bodies. This in turn deeply influences upper water layer heating, ecosystem dynamics (including primary productivity), and biogeochemical cycling [1]. Knowledge of the scattering and absorption properties of the water constituents is also of primary interest to estimate the concentrations of these constituents from in situ or satellite radiometric measurements, and to further delineate the global distribution and dynamics of aquatic life [2,3]. The investigation of the scattering properties of microalgae has also important implications to analyze and optimize the efficiency of photobioreactors for industrial purposes [4].

In opposition to the absorption process, the scattering process is directional inasmuch as it is a function of the angle between the incident light field and the scattered light, the so-called scattering angle. Knowing the directional scattering properties is, hence, highly informative for identifying the nature (i.e., size, shape, composition, structure) of the water constituents [5]. For convenience, the scattering properties are often expressed in terms of the volume scattering function (VSF), expressed in m^{-1} sr^{-1} and denoted β, which describes the angular distribution of light scattered by a small (conceptually infinitesimal) volume. The coefficient β can be expressed as follows:

#251344 Received 2 Oct 2015; revised 4 Dec 2015; accepted 4 Dec 2015; published 15 Dec 2015

$$\beta(\theta) = \frac{\partial I(\theta)}{E \partial r}, \quad (1)$$

where θ is the scattering angle, I is the radiance emerging from the scattering element illuminated by a collimated light beam of thickness r and irradiance E.

Despite its simple formulation, measurements of the VSF over the entire range of scattering angles (i.e., 0° to 180°) have been proved to be challenging, mainly due to the extremely large dynamic range of the signal (several orders of magnitude) over the full range of angles and to the difficulty to reduce and correct for stray light in the instrumental setup [6,7]. As a result, accurate measurements of $\beta(\theta)$ can only be achieved based on stringent requirements on the instrumental design and calibration, as well as protocols for data acquisition and processing [8]. In the past decades, measurements of the VSF for natural or phytoplankton cultures samples were scant [9,10]. Recently, new instruments using the last advances in optical technology have been developed to compensate for the lack of such important optical data [6,7,11–19]. Those instruments rely on different concepts and designs that inherently include different types of artifacts and error sources. Such instrument-related uncertainties might be evaluated from inter-comparison exercises, provided that all instruments are measuring identical samples.

In this study, an inter-comparison experiment was carried out using three VSF-instruments that are currently able to measure the VSF. Two of these instruments, namely the I-VSF [19] and the POLVSM [17] instruments, are prototypes which are not commercially available. The third one, namely the LISST-VSF [12] instrument, is commercially available. The goals of the inter-comparison experiment were (*i*) to compare the respective accuracies of those instruments and to highlight their respective strengths and complementarities, (*ii*) to document the directional scattering properties of various hydrosols, especially living algal cells that could further be used by the scientific community as a reference for radiative transfer calculations or phytoplankton cell modelling, and (*iii*) to ascertain the directional shape of the VSF of common phytoplankton species and mineral-like particles in the specific region of backward scattering angles which is of interest for ocean color satellite remote sensing. To achieve the inter-comparison exercise, a rigorous protocol was established to make sure that all concurrent measurements were performed for similar hydrosol compositions within the samples and to reduce any potential impacts of small detritus or bacteria/viruses from the phytoplankton-specific scattering properties at 515 nm.

The paper is organized as follows: section 2 describes the instrumental setup and the calibration methods adopted for each VSF-meter. The experimental protocol (e.g. sample conditioning) is outlined. Results and an uncertainty budget are reported in section 3. In section 4, the angular shape of the VSF of hydrosols (phytoplankton and mineral-like particles) is analyzed over the full range of scattering angle. Finally, tabulated values of the measured phase functions are provided in the Appendix.

2. Material and methods

2.1 Instrumental setup

2.1.1 I-VSF- HZG instrument

The prototype of the hyperspectral imaging VSF-meter, so-called I-VSF, was developed at the *Helmholtz-Zentrum Geesthacht* (HZG) [19,20]. The I-VSF design is based upon a combination of two reflectors, and permits a simultaneous determination of the VSF at a wide range of angles for a given wavelength [19]. The advantages of the I-VSF volume scattering meter are as follows: (*i*) for a single wavelength the scattering function from 8° to 172° at 1° intervals can be determined within a few seconds without changing the sensitivity of the detector (a CCD camera) and without moving any optical parts, and (*ii*) VSF can be

#251344 Received 2 Oct 2015; revised 4 Dec 2015; accepted 4 Dec 2015; published 15 Dec 2015

determined over the full visible spectrum (400-700 nm) with a spectral resolution of finer than 5 nm or for a tunable series of spectral bands.

The I-VSF system consists of a plasma lamp, a monochromator, a collimator, a sample chamber on top of a telescope as the detector optics, and finally a cooled CCD camera as the detector. The volume of the sample chamber is about 0.25 L and can be automatically stirred to avoid sedimentation of particle. The VSF is obtained by processing the image acquired by the CCD over a semi-circular slit that spans over the range of scattering angles for scattering originating from the middle of the sample flask. The actual angular resolution of scattering is 0.25°, although running means over 1° are applied to the functions to reduce the signal-to-noise level. A removable short pass filter protects the CCD from chlorophyll fluorescence light when illuminated with wavelengths <650 nm. At a single wavelength, such as 515 nm, the duration of a single scan made by the I-VSF instrument is less than 1 minute due to its design based on a camera.

2.1.2 LISST-VSF- Sequoia instrument

The LISST-VSF instrument (Sequoia Scientific, Inc.) [12] uses a combination of two methods to measure the VSF across a wide range of scattering angles, approximately from 0.1° to 150°. The range of angles from ~0.1° to ~15° is covered using a ring detector as in the LISST-100X instrument [21,22], while the angular range [15°-150°] is covered using a rotating eyeball detector. As it spins, the eyeball views scattering from different points along the beam (with corresponding different scattering angles). The single laser source is centered on 515 nm. The volume of the sample chamber used in the experiment was 2.25 L. Unfortunately, parts of the eyeball optical system had been damaged after intercontinental transportation from the US to the *Laboratoire d'Oceanographie de Villefranche* (France), where the laboratory inter-comparison experiment occurred, thus preventing us from having good quality data for scattering angle larger than 15° during the experiment. Therefore, all the results obtained from the LISST-VSF that are presented in the rest of the paper only concerns the VSF measured between 0.1° to 15°. The time to get a full VSF measurement for one scan using the LISST-VSF instrument is very short, typically few seconds. The final VSF was obtained by averaging over twenty scans for this instrument.

2.1.3 POLVSM- LOV instrument

The so-called POLarized Volume Scattering Meter (POLVSM) was developed at the *Laboratoire d'Océanographie de Villefranche* (LOV, France) to measure the 3x3 upper-right elements of the scattering Mueller matrix of hydrosols [17]. Multispectral measurements are carried out for an angular range from 1° to 179° with a resolution of 1°. An incident beam from a laser passes through an optical system (including polarizer, a beam expander and mirrors) to reach a first prism prior to entering a baffled chamber filled with the water sample (1.2 L). The direct light is removed after propagation over a path length of 7 cm thanks to a second customized prism. The second prism was designed to guide the direct light outside the basin and to avoid any undesired backscattered light arising from the prism surface. As a result, the detector only measures the scattering properties of the hydrosols. It is thus not necessary to apply any *a posteriori* correction of the signal received. The system allows collecting measurements for five wavelengths ranging from the violet to the near-infrared. At a single wavelength, the duration of a single scan acquired by the POLVSM instrument is about 10 minutes. Such a duration to acquire one scan is longer than the other instruments due to the concept of the POLVSM device and especially its ability to measure all the Mueller matrix elements.

2.1.4 Blank sample measurements and calibration

Measurements of "blank samples" (i.e., no hydrosols) were used to correct hydrosol measurements for the instrumental and water signals for the LISST-VSF and POLVSM

#251344 Received 2 Oct 2015; revised 4 Dec 2015; accepted 4 Dec 2015; published 15 Dec 2015

instruments (theoretical pure water VSF was used for the I-VSF). Thus, the VSF of the hydrosols contribution is retrieved by subtracting the blank measurements from the sample measurement. Blank measurements are carried out at the beginning of the experiment prior to entering any hydrosols in the sample chambers. The blank sample corresponds to ultrapure water (Milli-Q®) when hydrosols consist of microsphere beads or mineral-like hydrosols. The blank sample corresponds to artificial salt water when hydrosols consist of phytoplankton species.

The calibration method of the LISST-VSF and the POLVSM instruments is based on measurements of mono-disperse polystyrene micro-spheres (NIST traceable, Duke Standards™) of known refractive index and size. Calibration factors were calculated by matching raw measurements and theoretical results obtained through Mie theory calculations. In this study, 0.3-µm spheres were used for calibration; previous results showed that the volume scattering function is measured within ± 4.3% for the POLVSM instrument [17]. Regarding the I-VSF, geometrical correction and absolute calibration were carried out on the known VSF of a sample of pure methanol. Efficiency of the method was recently assessed on several monospecific phytoplankton cultures [11,19]. The various sources of errors that potentially exist for the I-VSF meter include inaccuracy estimate of the methanol calibration, averaging over different slit widths, and variability of beam attenuation related correction. Note that, in this study, the geometrical correction was also tested on 0.3-µm polystyrene spheres.

2.2 Protocol of the experiments

2.2.1 Protocol overview

A specific protocol was designed for the inter-comparison experiment (*i*) to ensure that all the instruments measure the same sample, especially in case of the optically fast changing algal cultures and (*ii*) to properly distinguish between the contribution of phytoplankton from the contribution of the potential presence of sub-micron detrital matter or bacteria/viruses within the biogenic samples. Figure 1 summarizes the different steps required to measure the VSF of hydrosols. First, concentrated phytoplankton cultures or mineral-like hydrosols were diluted to get reasonably low concentrations to prevent a multiple scattering regime within the sample chambers of the VSF instruments. The hydrosol concentrations and size distributions of each diluted sample were systematically checked using a MultiSizer™ 3 COULTER COUNTER® and from acquisitions of ancillary optical data (absorption and attenuation coefficients). The attenuation coefficient was acquired using the LISST-VSF, as well as a laboratory transmissiometer, and the absorption coefficient using a point-source integrating-cavity absorption meter (PSICAM) [23]. Then, aliquots of the dilution were placed in the sample chamber of each VSF instrument. Full records of these measured parameters are required to interpret measurements in terms of number and concentration of particles (beads, cells, dust-like hydrosols). It should be highlighted that a gentle stirring was made for two of the three VSF instruments, namely the LISST-VSF and the I-VSF, during the measurements. Note that the validation and the application of each instrument that was performed in previous studies [12, 17, 19] already showed that the instruments manage to handle pretty well to reduce the influence of settling of particles or aggregation of particles during a scan. Ancillary data must also be acquired to process the raw measurements of the different VSF-meters. In particular, knowledge of the attenuation coefficient is needed to correct for the optical path length in the sample chamber of the instrument. As phytoplankton cells were collected during the exponential growth phase and removed from the culture chamber, they can change in size, shape and optical properties during the experiment, all the ancillary and VSF measurements were acquired concurrently.

To make sure that the phytoplankton scattering properties were isolated from other possible sources of scattering (e.g., detrital matter, bacteria or viruses), the axenic conditions

#251344 Received 2 Oct 2015; revised 4 Dec 2015; accepted 4 Dec 2015; published 15 Dec 2015

of the algae samples were tested. Therefore, the hydrosol samples were filtered through glass-fiber filter (GF/F, Whatman; collecting 99% of all particle >0.5µm) just after the VSF measurements. The above measurements were then repeated for the sample filtrate. In case of an algal culture, a significant difference between the blank sample measurements and the filtrate measurements indicates that some matter (i.e., detritus, bacteria, viruses) other than algal cells was present in the initial algal samples. In this study, the filtrate measurements were considered as "blanks" and subtracted to obtain the proper scattering signature of the algal cells only for all algae.

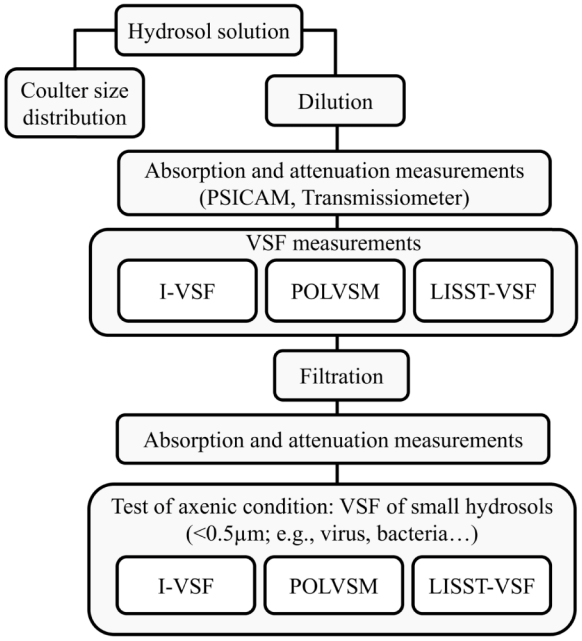

Fig. 1. General overview of the protocol of the inter-comparison laboratory experiments between POLVSM (LOV), I-VSF (HZG), and LISST-VSF (Sequoia) instruments.

2.2.2 Ancillary data

Laboratory transmissometer measurements

To pre-determine the optimal particle concentration and to perform corrections of the VSF-instruments raw data, the spectral beam attenuation coefficients of the samples were measured using a standard beam transmission set up as described by Tan [20]. The light source is a laser-driven plasma lamp (Eq. (99-)LDPS; Energetic Technology, USA). The light of the lamp is coupled into an optical fiber and is then collimated using a lens-pinhole system. In a distance of 40 cm, the light beam passes another pinhole and impinges on the diffusor window of a hyperspectral irradiance sensor (RAMSES-ACC; TriOS, Germany) that is used for the spectral light intensity measurements. Due to the collimation and the distances, the acceptance angle of the detecting system is 0.85°. A glass cuvette of path length 0.15 m (DURAN Group, Germany) containing the water sample is placed in the beam. Milli-Q® water is used as a reference. The attenuation coefficient $c(\lambda)$ (m^{-1}), is derived from the ratio of I/I_0 as follows $c = -\log_n(I/I_0) / 0.15$ m, where I is the light intensity when the cuvette is filled with the sample and I_0 is the light intensity when the cuvette is filled with Milli-Q® water. The attenuation measurement is repeated several times (typically 3 to 5) to get an uncertainty estimate. Differences in attenuation (scattering and absorption) by pure water induced by the salinity of the sample water are corrected using published correction coefficient [24,25]. Temperature differences were small and the effect on attenuation could be neglected.

#251344 Received 2 Oct 2015; revised 4 Dec 2015; accepted 4 Dec 2015; published 15 Dec 2015

Absorption measurements

Hyperspectral measurements of the light absorption coefficient of the hydrosols were carried out using a Point-Source Integration Cavity Absorption Meter (PSICAM) [23]. The absorption coefficient, $a(\lambda)$ (m^{-1}) is determined from the measurements of the sample and a pure water reference. Any effects of the absorption of pure water induced by difference in temperature and salinity between sample and reference were corrected [26]. All measurements are carried out three times. The particulate scattering coefficient, b_p, is finally simply calculated by subtracting the absorption coefficient from the attenuation coefficient c.

2.3 Samples

2.3.1 Phytoplankton cultures

Five monospecific cultures of marine phytoplanktonic algae were analyzed (Table 1). Several criteria were used to select the phytoplankton species. First, it was important to cover several phytoplankton groups that are often encountered in the ocean. Therefore, a variety of phytoplankton species that belong to several phytoplankton groups such as diatoms, dinoflagellate or green algae was selected. Second, it was of interest to account for a variability in the general shape of the species to examine the potential influence of the shape of species on the VSF. Therefore, species having a shape ranging from a spherical-like shape to cylindrical-like shape (i.e., strongly not spherical) were selected. Third, small single cells phytoplankton (i.e., nanophytoplankton) were mostly used to reduce as best as possible during this study potential settling of cells within the sample. Settling process could happen rapidly when large cells are used. Thus, the species had been selected to be representative of the nanophytoplankton type whose typical cell diameters are comprised between 2 and 20 µm. However, we are aware that further experiments should be carried out in the near future using larger sizes of phytoplankton species (i.e., microphytoplankton) which will allow getting closer to blooming phytoplankton conditions. Stock cultures of *Chlorella autotrophica* [27], *Cylindrotheca closterium* [28] and *Dunaliella salina* [29] were provided by the service Culture of Marine Phytoplankton at LOV (France), while those of *Karenia mikimotoi* [30] and *Skeletonema cf. costatum* [31] by the Roscoff Culture Collection (RCC, Brittany, France). The phytoplankton cells were diluted in isotonic solution (artificial seawater of 35 psu) to avoid degradation of the cells by osmosis.

The LOV cultures were grown in batch using F/2 medium. The medium was autoclaved and filtered using a 0.2-µm hydrophilic polypropylene membrane (GHP). Cultures are incubated at 21°C with constant illumination of 100 µmol photons m^{-2} s^{-1} under a 14:10 dark:light cycle. Cells were maintained in exponential growth conditions until cell concentration was appropriate for optical measurements. All the cultures were regularly treated with antibiotics to remain as close as possible to axenic conditions. With regard to RCC cultures, the medium used was prepared from seawater collected offshore Roscoff city (salinity ca. 33‰), stored for at least two months in darkness, then filtered on 0.22-µm filters (Millipore filter GSWPO9000 plus Millipore prefilter AP1507500) and autoclaved. All RCC strains were exposed to a 12H/12H day/night light cycle provided by "daylight" fluorescent tubes (Tabur-Neons Sylvania Daylight F58W/54/765). Light intensity for culture maintenance did not exceed 100 µmol photons m^{-2} s^{-1}.

The particle size distribution measurements of each sample were performed with the Coulter counter just before the optical VSF measurements. In this manner, phytoplankton cells were supposed to be equilibrated with the sample volume in terms of osmosis and hydration preventing any change in size between Coulter counter and optical measurements. Table 2 gives the different parameters of interest to characterize the particle size distribution of each sample. It is worth noting that the size parameters (e.g., effective radius) of *C. closterium* are given in terms of equivalent spherical dimension whereas this species is highly elongated with a length-to-width ratio of almost 10. Figure 2 shows the particle size

#251344 Received 2 Oct 2015; revised 4 Dec 2015; accepted 4 Dec 2015; published 15 Dec 2015

distribution for all the species studied in our experiment. Despite the fact that most of the phytoplankton species exhibited a dominant mode in their size distribution, a polydispersion is observed. Note that a monodispersed distribution would have implied a very narrow peak of the particle size distribution around a single value of the particle diameter. It is interesting to highlight that the hydrosols remain polydispersed when the size is greater than 0.5 µm, which means that the removal of the filtrate blank measurement to the total VSF measurement do not alter the polydispersion of the hydrosols within the samples. *C. autotrophica* exhibited two distinctive major size modes centered on 2 and 4 µm, respectively. It is thus likely that *C. autotrophica* species was in mitosis during the time of the experiment with parent cells of twice the size of daughter cells. However, biological measurements relying on the internal structure of *C. autotrophica* were not available to confirm rigorously this assumption.

Table 1. Summary of phytoplankton characteristics that are analyzed in this study.

Species	Strain	Algal Class	Common class	Shape
Chlorella autotrophica	CCMP243	Chlorophyceae	Green algae	ovoid/spherical
Cylindrotheca closterium	AC170i	Bacillariophyceae	Diatoms	fusiform, lanceolate
Dunaliella salina	CCAP19118	Chlorophyceae	Green algae	ovoid
Karenia mikimotoi	RCC1513	Dinophyceae	Dinoflagellate	spherical
Skeletonema cf. costatum	RCC1716	Bacillariophyceae	Diatoms	pennate, cylindrical

Table 2. Particle size distribution parameters of the hydrosols as measured by Beckman-Coulter counter: r_g and v_g are mean radius and variance, r_{eff} and v_{eff} are the effective radius and variance, respectively. Absorption (a) and particulate scattering (b_p) coefficients at 515 nm as retrieved from the PSICAM and transmissiometer measurements are reported as well.

Sample	Particles (cm^{-3})	r_g (µm)	v_g (µm)	r_{eff} (µm)	v_{eff} (µm)	a (m^{-1})	b_p (m^{-1})
C. autotrophica	4996.8	1.47	0.18	2.01	0.23	0.049	3.534
C. closterium	2747.9	1.13	1.35	3.52	0.07	0.131	3.343
D. salina	2188.7	1.87	1.40	5.34	0.03	0.277	0.523
K. mikimotoi	1234.5	3.14	0.77	9.32	0.33	0.103	0.699
S. cf. costatum	2254.4	0.95	2.12	4.89	0.14	0.347	1.904
Arizona dust	2398.9	1.16	0.55	3.27	0.65	0.035	2.864

2.3.2 Mineral-like hydrosols

One sample of this study contained an irregular-sized mineral-like suspension of Arizona Test Dust (Powder Technology, Inc., "PTI"). This particle standard is an irregular mineral dust size-sorted from ISO-12301-1 test powders. Particle size distribution of the dry dust fraction measured here follows a lognormal distribution within a size range of 2 to 4.5 µm (5th and 95th percentiles) as provided by the manufacturer. They are dominated by SiO_2 (68–76% mass) and Al_2O_3 (10–15% mass), with refractive indices (real part) of ~1.55 and ~1.76–1.78, respectively. The imaginary part of refraction for the Arizona Dust cannot be assumed negligible as demonstrated by a low but non-null absorption coefficient measured during the experiment (Table 2). A small volume of dust aerosols was diluted in 5 L of Milli-Q® water to yield an attenuation coefficient ranging over wavelength between 2 and 3 m^{-1}. To ensure the good dispersion of these dust-like hydrosols, the sample was passed to an ultrasonic device and a small amount of dispersant (sodium hexametaphosphate) was added. Note that sodium hexametaphosphate solution showed no significant scattering contribution in comparison to the Milli-Q® blank.

#251344 Received 2 Oct 2015; revised 4 Dec 2015; accepted 4 Dec 2015; published 15 Dec 2015

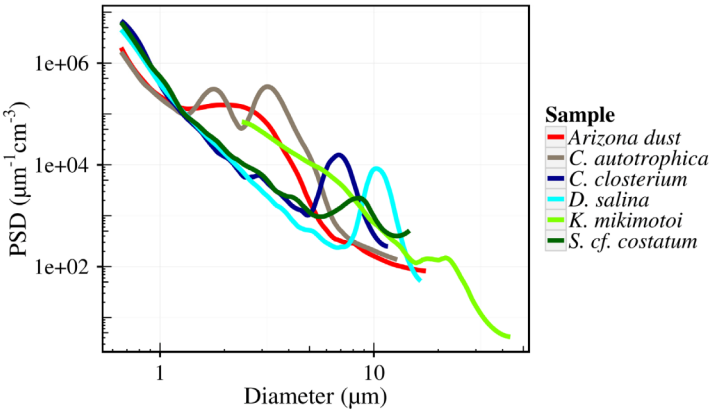

Fig. 2. Particle size distribution (PSD) of the hydrosols analyzed during the experiment obtained from the particle number concentration measured by Coulter counter.

3. Results

In the framework of the inter-comparison experiment described in this paper, a focus was put on VSF data acquired at 515 nm which is the common wavelength of the three VSF instruments.

3.1 Validation with polystyrene microspheres

Suspensions of mono-disperse polystyrene microspheres (NIST traceable, Duke Standards™) of 3 µm in diameter were used to verify the consistency of the measurements acquired by the different volume scattering meters instruments with theory. Note that the beads of 3 µm exhibit significantly different scattering properties than the beads of 0.3 µm used for calibration thereby making the validation comparison meaningful. The same concentration of 3-µm beads was used for all the instruments, thus, permitting inter-comparison of the different devices. Microspheres beads were first added to Milli-Q® water and then ultrasonicated prior to entering the instrument sample chambers.

The results of the VSF-meters are compared with the theoretical phase function of the beads computed using Mie theory [32]. For that purpose, VSF measurements (in m^{-1} sr^{-1}) are divided by the scattering coefficient b_p (in m^{-1}) to get the phase function (in sr^{-1}). Following the manufacturer specifications for these beads, a log-normal size distribution with a mean radius of 1.50 ± 0.01 µm and a refractive index of 1.20 (relative to water) was used for Mie calculations. Figure 3 shows the comparison of the directional shape and amplitudes of the phase functions between the measurements and simulations. A satisfactory overall consistency is observed between Mie theory and the three VSF-meters. In particular, the normalized root mean square difference (NRMSD), which is informative on the relative difference between measurements and theory over all the scattering angles, shows values of 13.1%, 3.1% and 3.1% for LISST-VSF, I-VSF and POLVSM instruments, respectively. The I-VSF and POLVSM phase functions exhibit a strong agreement for angles larger than 25°, especially at backward angles which are of primary importance for the analysis of the backscattering properties of hydrosols. However, it should be highlighted that an overestimation of the phase function measured by the I-VSF data can be noticed for scattering angles lower than 25°. The I-VSF instrument uses a neutral density filter in this range of angles for attenuating the strong signal of the forward scattering light. Tan et al. [19] already showed that an adjustment procedure is necessary for the I-VSF instrument to overcome possible overestimation of the measurements. They also pointed out that the adjustment procedure is not really applicable to polystyrene beads samples for which the VSF varies very rapidly with the scattering angle. However, they showed that the adjustment procedure is

#251344 Received 2 Oct 2015; revised 4 Dec 2015; accepted 4 Dec 2015; published 15 Dec 2015

clearly applicable in the case of natural hydrosols (phytoplankton or mineral-like particles) for which the angular variation of the VSF is smoother with angles (i.e., monotonically decreasing with scattering angles). As a result, the overestimation observed in Fig. 3 for the beads sample using the I-VSF instrument at angles lower than 25° does not alter the measurements that will be presented later in the paper about the phytoplankton and mineral-like hydrosols.

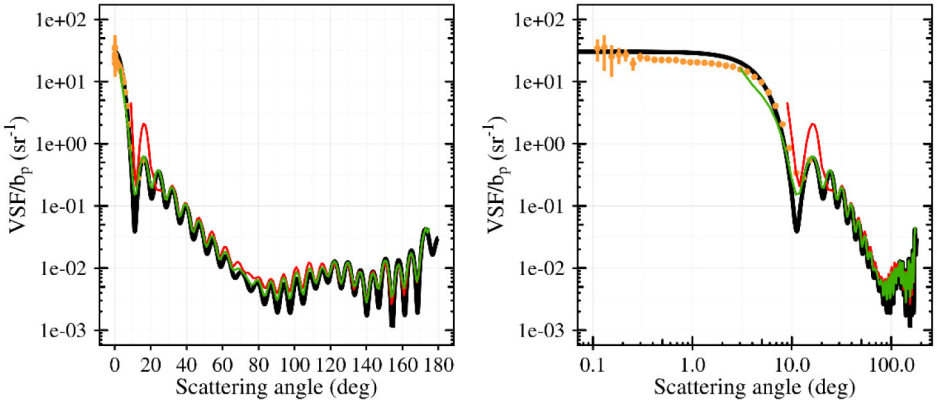

Fig. 3. Comparison in semi-log and log-log scale of the I-VSF (red line), LISST-VSF (orange dots) and POLVSM (green line) phase function (i.e. VSF/bp) with Mie theory (black line) based on 3-µm polystyrene beads.

3.2 Angular shape of the VSF

As mentioned earlier, volume scattering functions of five algal samples (i.e., cultures of phytoplanktonic species) and one mineral-like hydrosol sample (Table 1 and Table 2) were measured by the three VSF-meters as a function of the scattering angle. Figure 4 shows the VSF data of the hydrosols in physical units (i.e., m^{-1} sr^{-1}). To quantify the overall contribution of the filtrate blank VSF to the total VSF (i.e., the total VSF is the VSFs measured prior to filtering the sample through the GF/F Whatman filter), the ratio between the scattering coefficient of the filtrate blank sample and the scattering coefficient of the total VSF was calculated for each species. The results show that the filtrate blank contributes by 9.8%, 1.3%, 15.8%, 13.1% and 0.9% to the total VSF for the species *C. autotrophica, C. closterium, D. salina, K. mikimotoi* and *S. cf. costatum*, respectively. Therefore, the amplitude of the signal induced by the residual hydrosols (i.e., filtrate blank) remains significantly weaker than that induced by phytoplankton. This means that residual hydrosols like detritus or bacteria did not alter significantly the sample thus providing us with confidence that the VSF of algal cells only was effectively measured. Note also that the angular shape of the filtrate blank does not influence significantly the VSFs of phytoplankton species including in the backscattering region as it will be shown later in the manuscript (see Fig. 4).

#251344 Received 2 Oct 2015; revised 4 Dec 2015; accepted 4 Dec 2015; published 15 Dec 2015

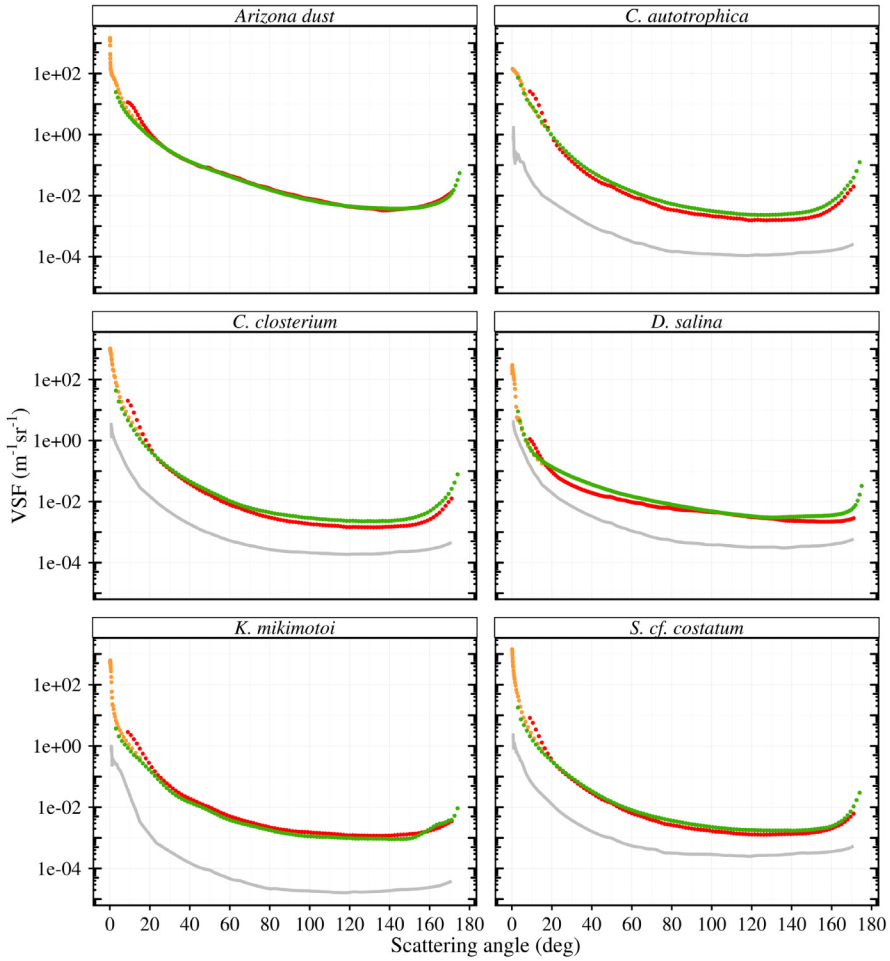

Fig. 4. Volume scattering functions (VSF) in m^{-1} sr^{-1} measured by the I-VSF (in red), LISST-VSF (in orange) and POLVSM (in green) instruments for all the samples, namely, the mineral-like sample (Arizona dust) and the five different algal samples. Filtrate measurements of VSF (blanks) are also shown (grey lines) for phytoplankton species (i.e., Arizona dust particles are not biogenic so, this sample was not filtrated).

An overall agreement in between the three instruments can be readily observed for the six samples. First of all, LISST-VSF and POLVSM measurements systematically overlap satisfactorily at small scattering angles (up to 15°) where the measured signal is the strongest. At larger angles, where signal intensity is smaller by several orders of magnitude than that of the near forward peak, the angular shape of the measured VSF is similarly retrieved by the I-VSF and POLVSM instruments. This is especially interesting at the backward angles >150° where a significant increase of the VSF is observed for most algal samples; such an increase reached 1.5 order of magnitude for *C. autotrophica*, *C. closterium*, and *S. cf. costatum* (Fig. 4). Note, however, that the amplitude of the VSF for the *C. autotrophica* measured by the POLVSM device is higher than that measured by the I-VSF instrument. Since the VSF data are calibrated in physical units, it is likely a magnitude difference. To check this assumption, the VSF data of *C. autotrophica* were normalized to their integrated value over the angular distribution available for each instrument for both instruments (Fig. 5). It is observed from Fig. 5 that the angular shape of the VSF beyond 150° is similar for I-VSF and POLVSM data, thus confirming that the differences between the two instruments as observed in Fig. 4 for this

#251344 Received 2 Oct 2015; revised 4 Dec 2015; accepted 4 Dec 2015; published 15 Dec 2015

species are magnitude differences. The difference in the amplitude observed between I-VSF and POLVSM instrument for *C. autotrophica* is likely due to differences in cell concentration between the samples contained within the I-VSF and POLVSM chambers. Despite the care brought to the protocol to rigorously measure the same algal sample using each instrument, it is worth reminding here that cells in the *C. autotrophica* sample could likely be in the process of mitosis during the laboratory experiment as suggested by the presence of two modes in the size distribution measurements (see section 2.3.1). Since the full series of acquisitions by the POLVSM device takes longer than the time needed by the I-VSF instrument, it is likely that it might have left sufficient time for cell division of *C. autotrophica* within the POLVSM chamber. As a result, the number of cells probably increased leading to an enhancement of the amplitude of the VSF measured by POLVSM as observed in Fig. 4. It is interesting to note that Fig. 5 also reveals that the angular shape of the filtrate sample varies by less than a factor of 2 from 150° to 178° while it varies by more than one order of magnitude for both I-VSF and POLVSM data. As a result, the angular shape of the filtrate data beyond 150° does not influence significantly the angular increase of the VSF of the phytoplankton species. Note that similar results are obtained for the other species.

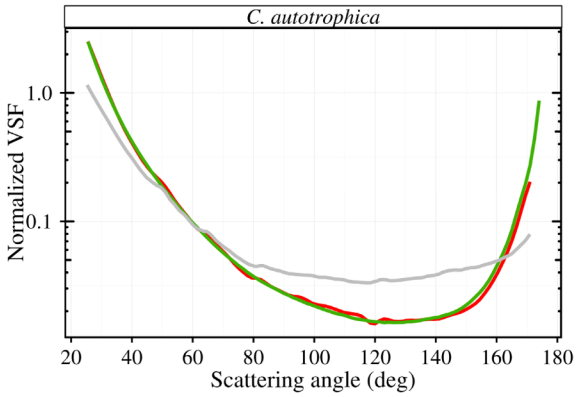

Fig. 5. Normalized volume scattering functions (VSF, in sr^{-1}) of the species *C. Autotrophica* measured by the I-VSF (in red) and POLVSM (in green) instruments. The normalized VSF was calculated by dividing the VSF by the integrated value over the angular distribution available for each instrument. Filtrate measurements of VSF (blanks) are also shown (grey lines) for this species.

From a quantitative point of view, the relative standard deviation for a given scattering angle θ, noted *rSTD(θ),* has been calculated to determine the percent residual difference of the instrument VSFs from average curve as a function of angle (Fig. 6(a) and Fig. 6(b)). *rSTD(θ)* is calculated as follows [Eq. (2)]:

$$rSTD(\theta) = \frac{1}{\overline{VSF}(\theta)} \sqrt{\frac{1}{N_{instr}} \sum_{instr} \left(VSF(\theta, instr) - \overline{VSF}(\theta) \right)^2}, \qquad (2)$$

where $VSF(\theta,instr)$ is the VSF value acquired by a given VSF-meter, N_{instr} is the number of instruments, $\overline{VSF}$ is the mean VSF averaged over the data sets acquired by the instruments available at the given angle.

The variation of *rSTD(θ)* with the scattering angle show that the percent residual difference between the three instruments ranges from a few percents to about 60% depending on the scattering angle. The largest differences, typically between 40% and 60%, are observed at low values of θ (i.e., near the forward peak) and at high values of scattering angles (i.e., backscattering region) for given species only (e.g., *C. Autotrophica*, *C. Closterium, D. Salina)*. However, it should be highlighted that the absolute calibrated values of the VSF

#251344 Received 2 Oct 2015; revised 4 Dec 2015; accepted 4 Dec 2015; published 15 Dec 2015

remain very weak in the backscattering region (about 10^{-2} m^{-1} sr^{-1} as shown in Fig. 4) which could tend to artificially increase the value of the percent relative difference *rSTD(θ)* at these angles. As already suggested from Fig. 4, the percent residual difference does not show any pronounced trend of variation with scattering angles. It could be noticed as well that the lowest discrepancy between the three instruments is observed for the Arizona dust sample.

In addition to the calculation of *rSTD(θ),* the mean relative standard deviation (noted $rSTD_{mean}$) has also been calculated over the data sets acquired by the three instruments. The $rSTD_{mean}$ values are informative for the overall uncertainty associated with the VSF measurements. $rSTD_{mean}$ is obtained by averaging *rSTD(θ)* over the full range of scattering angles (Fig. 6(c)). The value of $rSTD_{mean}$ is around 10% for the mineral-like hydrosols sample against 18% to 25% for the samples of the phytoplankton species (Fig. 6(c)). A higher variability could be expected for the sample of phytoplankton species since algal cells might divide, reorganize their internal structure or shape during data acquisition. It is likely as well as settling of particles or motile particles might contribute to the uncertainties observed in Fig. 6(c). However, it is difficult to confirm this latter assumption since we do not have the required measurements for that. Figure 6 finally reveals that it is more difficult to measure the angular scattering properties of living hydrosols than those of mineral-like hydrosols.

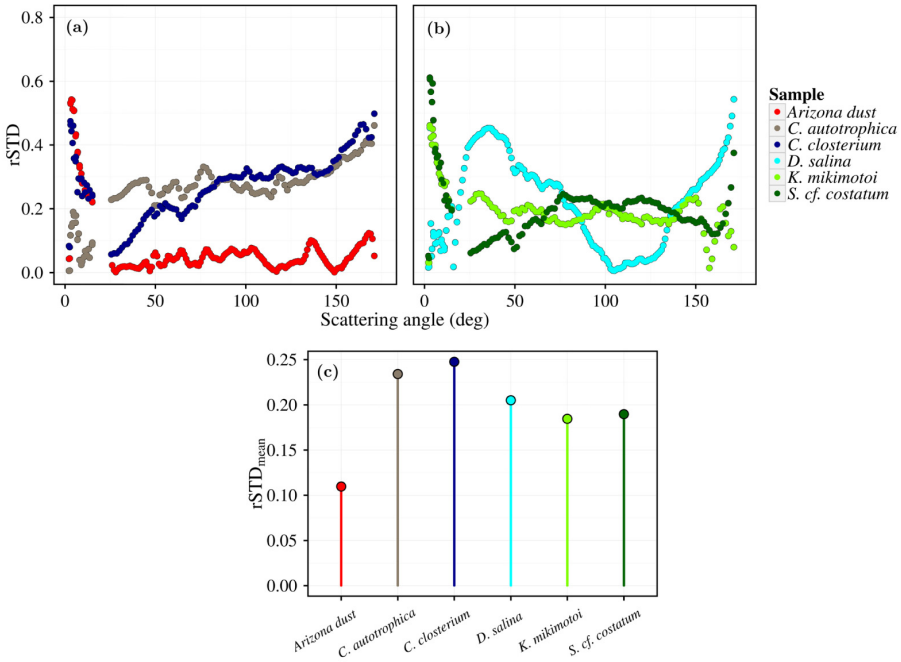

Fig. 6. Relative standard deviation *rSTD(θ)* between VSF measurements of each instrument and the VSF averaged over the three instruments as a function of angle (a) for the hydrosols *Arizona dust*, *C. Autotrophica*, *C. Closterium*, (b) for the hydrosols *K. Mikomotoi*, *D. Salina* and *S.cf., costatum*; (c) mean relative standard deviation ($rSTD_{mean}$) calculated over the scattering angles for each hydrosol sample.

Since the I-VSF, LISST-VSF and POLVSM are based on different instrumental concepts, it can be safely thought that artifacts in calibration are uncorrelated between the three instruments. Therefore, averaging the instrument-related VSF should smooth error measurements and decrease data uncertainty. For this reason, the VSF averaged over the three instruments will be discussed in the rest of the paper. Furthermore, the tabulated values of the respective phase functions (i.e., VSF/ b_p) are provided in Appendix to make those data publicly available for further consideration.

#251344 Received 2 Oct 2015; revised 4 Dec 2015; accepted 4 Dec 2015; published 15 Dec 2015

3.3 Angularly integrated values and uncertainties

The integration of the VSF over all or backward scattering angles provides the particulate scattering (b_p) and backscattering (b_{bp}) coefficients, respectively. These coefficients are commonly used in ocean optics to relate the water-leaving radiance to optical properties and eventually to biogeochemical parameters related to the water constituents. b_p and b_{bp}, are directly related to the VSF, $\beta(\theta)$ by Eq. (3) and Eq. (4):

$$b_p = 2\pi \int_0^{\pi} \beta(\theta) \sin\theta d\theta, \quad (3)$$

$$b_{bp} = 2\pi \int_{\pi/2}^{\pi} \beta(\theta) \sin\theta d\theta. \quad (4)$$

The b_p was derived by numerically integrating the VSF measurements over the full angular range [Eq. (3)] using a nearest-neighbor approach for the values at the extreme angles which are outside of the measured angular range. The derived b_p are compared in Fig. 7 with those measured using the combination of the PSICAM and a transmissiometer (section 2.2.2) for the algae and mineral samples as well as standard polystyrene beads of 0.3 and 3 microns. Those two data sets are highly correlated (R^2>0.96) with a slope of the regression line (dashed line) of 1.15 when all the measured samples are taken into account. The highest discrepancy between b_p derived from the VSF and b_p derived from *c* - *a* is observed for *C. autotrophica* species. As mentioned earlier, the potential cell division may have enhanced the VSF of *C. autotrophica*. Since b_p measurements that were carried out by the transmissiometer/PSICAM were performed about 1 hour before the full VSF acquisition, it is likely that the potential cell division alter significantly the number of cells which in turn could induce higher values of b_p derived from VSF data relatively to the *c* - *a* data. The changes in the conditions of the experiment for *C. autotrophica* between the VSF and *c* - *a* measurements do not allow an optimal inter-comparison of the data. Therefore, the data corresponding to *C. autotrophica* species were removed for the purpose of the inter-comparison. The new determination coefficient value R^2 is then around 0.99 with a slope of the regression line (continuous line) of 0.98; the corresponding value of the root-mean-square error (rmse) is 0.11 m^{-1}. Those values clearly point out good agreement (within 2%) between b_p derived using VSF meters and that derived from *c* - *a* data. These results highlight the performance of the VSF instruments for deriving the particulate scattering coefficient.

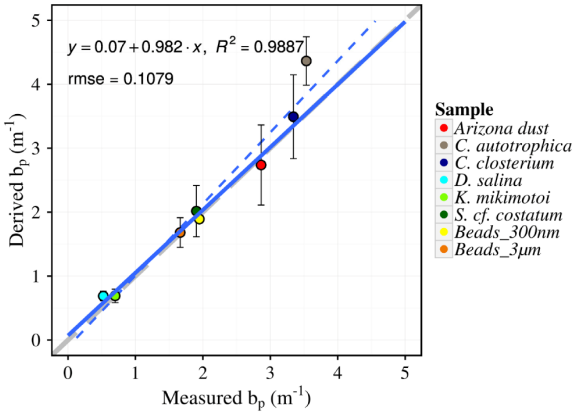

Fig. 7. Comparison of the particulate scattering coefficient b_p measured from the combination of transmissiometer/PSICAM instruments (x-axis) with b_p derived from angular integration of the VSF (averaged over the three VSF meters instruments). Equation of the regression line (blue lines), coefficient of determination (R^2) and root-mean-square error (rmse) are given in the upper left part. Note that the data obtained for the species *C. autotrophica* were not taken into account to establish the equation of the regression (solid blue line, see text).

#251344 Received 2 Oct 2015; revised 4 Dec 2015; accepted 4 Dec 2015; published 15 Dec 2015

The particulate backscattering ratio $\tilde{b}_{bp}$, which is defined as the ratio between the backscattering and scattering coefficients b_{bp}/b_p. is an important parameter for the characterization of hydrosols [33]. It is often used in radiative transfer models [34] since this parameter is independent of the hydrosols concentration. In addition, it is informative of the overall angular shape of the phase function. For these reasons, it is more relevant to compare the backscattering ratio $\tilde{b}_{bp}$ derived from the I-VSF with that derived from POLVSM measurements rather than to compare the sole particulate backscattering coefficient b_{bp}. Figure 8 shows the results of this comparison. A strong correlation is observed (R^2~0.99). The slope of the linear regression shows a departure of 4% from the 1:1 line. All the phytoplankton species exhibit $\tilde{b}_{bp}$ values lower than 0.012 except for *D. salina* ($\tilde{b}_{bp}$ = 0.033) which is in accordance with compiled values from the literature [35–37]. Beyond the analysis of the respective backscattering ratio with the type of hydrosols, the comparison of Fig. 8 shows that the uncertainty attached to the derivation of $\tilde{b}_{bp}$ is about 0.0018 corresponding to 3.7% relative error over the measured range.

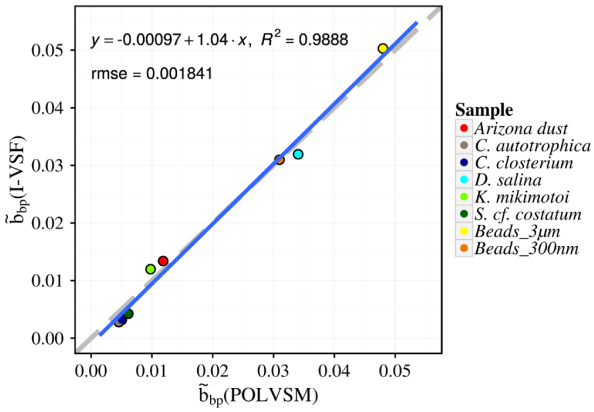

Fig. 8. Comparison of the backscattering ratio $\tilde{b}_{bp}$ as derived from the POLVSM and the I-VSF instruments, for all the samples and for the standard beads.

4. Discussion

4.1 Phase function features at backward angles

The most commonly used phase function of hydrosols for radiative transfer computations and for the development of inverse algorithms rely on the Fournier-Forand (FF) parametrization [38]. The FF parameterization is based on approximation of Mie theory to provide a theoretical approach to model the VSF when measurements are not available. The FF phase function is calculated for a given refractive index and Junge power-law particle size distribution exponent. Practically, the FF phase function is obtained by setting a desired value of the backscattering ratio following the method described in [34]. Here, the FF parameterization is used to analyze the angular features of the phase functions measured during our laboratory experiment.

Figure 9 shows the comparison of the measured phase functions with those derived from the FF parameterization having a similar backscattering ratio $\tilde{b}_{bp}$ as that obtained from the VSF measurements. The refractive index and the Junge exponent used in the FF parameterization to get $\tilde{b}_{bp}$ are also indicated in Fig. 9. For comparison, the Petzold's measurements [9] of the phase functions obtained for clear, coastal and turbid waters are also

#251344 Received 2 Oct 2015; revised 4 Dec 2015; accepted 4 Dec 2015; published 15 Dec 2015

superimposed only when their respective $\tilde{b}_{bp}$ values are close to that of our measurements (i.e., Arizona dust, *D. salina*, *K. mikimotoi*). The $\tilde{b}_{bp}$ of the Petzold's measurements are 0.0443, 0.0134, 0.0199 for clear, coastal and turbid conditions, respectively. Note that no measurements were done beyond 170° by Petzold [9].

It can be readily observed that a strong consistency between measurements and FF parameterization is obtained for the majority of the samples for a large range of scattering angles, typically from the forward peak up to 150°. In this range of scattering angles, theoretical phase functions nicely match measurements. However, a significant difference is observed between 30° and 90° for the Arizona dust where the FF phase function underestimates the measurements. Significant differences between FF phase functions and measurements are observed for scattering angles greater than 150° for all samples (Fig. 9). In particular, the measured phase functions exhibit a pronounced increase beyond 150°. Such an increase is totally absent in the FF approximations, which show a flat angular shape. It has been shown in Fig. 4 that the increase of VSF observed in the measurements is not due to instrumental artifacts but more likely to optical features of the hydrosols. It is worth noting as well that such a specific pattern was observed earlier for phytoplankton [19,39,40] or other living cells [41]. It is important to highlight that the comparison of the VSF measured here with the Fournier-Forand phase functions makes sense because the particle size distribution of the hydrosols shows that polydispersion does exist within our sample, as observed in Fig. 2. Indeed, one could think that the removal of small particles through the subtraction of the filtrate blank from the VSF measurements could lead to a strongly monodispersed size distribution of the hydrosols. In addition, Fig. 4 pointed out that the angular shape and the magnitude of the VSFs measured for the filtrate blank sample do not significantly influence the increase of the signal at high scattering angles. Therefore, particles smaller than 0.5 µm do not necessarily contribute to flatten the shape of the VSFs when larger hydrosols such as phytoplankton species similar as those studied here are present in the sample. Our study does not allow confirming that a sharp increase of the VSFs would be observed in natural waters composed of polydispersed hydrosols or in blooming conditions (i.e., major size mode of phytoplankton). However, past and recent studies about VSFs measurements that were performed in natural waters [11,40,42] showed that a significant increase of the VSF in the backward direction at angles greater than 150° could be observed despite the fact that hydrosols could be strongly polydispersed. Those studies thus tend to corroborate the fact that the increase of VSF at high angles as obtained during our laboratory experiment could be realistic.

The fact that the FF approximation is not able to reproduce satisfactorily the directional patterns in the backscattering region suggests that potential errors could be made when computing the water leaving radiance from radiative transfer models. Indeed, the increase of the backward VSF at angles greater than 150° can significantly impact the directional distribution of underwater and backscattered light [43,44]. Interestingly, it was shown in a previous study that similar increases of the phase function at large scattering angles, as those observed here in our data, might be retrieved theoretically, provided that simple internal structures of the cells are taken into account when modeling hydrosols optical features [45]. Further studies are therefore required to improve modeling of phytoplankton internal structure to better represent the increase of VSF at large scattering angles. The VSF measurements that were acquired in our study are one step in that direction. Laboratory and field measurements of phytoplankton-specific VSF need to be continued in the future to properly document the natural variability of the directional effects of the hydrosols at backward angles. Note finally that the comparison of the measurements with Petzold's phase functions shows a good agreement, thus confirming the relevant use of Petzold measurements for modelling purposes, despite the fact that Petzold data were acquired on a small number of natural samples.

#251344 Received 2 Oct 2015; revised 4 Dec 2015; accepted 4 Dec 2015; published 15 Dec 2015

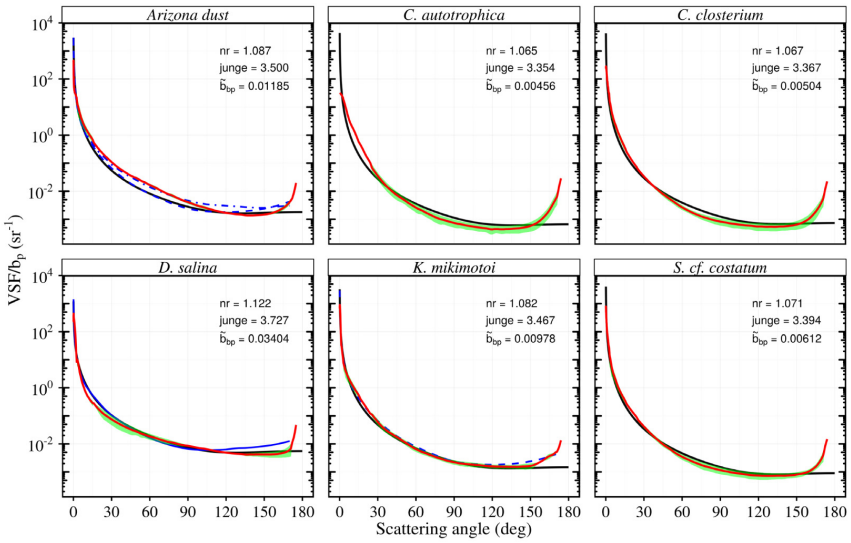

Fig. 9. Comparison of the phase function measured using the VSF averaged over the three VSF meters (in red) with the Fournier-Forand (FF) phase function (in black). Note that FF phase function has been calculated for a value of the backscattering ratio that is similar as those obtained from the measurements. The 2-standard-deviation interval that is related to the measurements is shown in green. The refractive index (nr) and the Junge power law exponent that are used to compute the FF phase functions are also reported. The Petzold's phase functions are also shown in blue for clear (solid), coastal (dash) and turbid (dot-dash) conditions for hydrosols samples having similar backscattering ratio, namely, Arizona dust, *D. salina*, *K. mikimotoi* (see text for details).

4.2 Retrieval of the particulate backscattering coefficient from VSF measurements at a single angle

As described in Eq. (4), the best way to determine the particulate backscattering coefficient, b_{bp}, consists of integrating the VSF over the backward scattering angles. However, measurements of the VSF over the entire backward hemisphere remain a challenging task in the field (ocean, lakes, rivers…), especially because of the complex deployment of most of the current instruments that are capable of measuring the full VSF. Because of this, Oishi [46] used the mean value theorem to introduce a conversion factor, denoted as χ_p, to relate b_{bp} with the VSF measured at a single scattering angle. The χ_p factor is simply defined as:

$$\chi_p(\theta) = \frac{b_{bp}}{2\pi\beta(\theta)}. \quad (5)$$

Note that many studies showed that the factor χ_p exhibits the least variability around the scattering angle value of 120° [35,40,47,48].

The χ_p factors were derived from the VSF measurements of I-VSF and POLVSM instruments and then averaged for each sample. The mean χ_p factors are compared with those obtained from the literature in Fig. 10. As shown in Fig. 2, the particle size distribution of the sample shows polydispersion. Thus, it makes sense to compare our measurements with previous data collected in natural waters. The angular variability of χ_p factors for phytoplankton samples is fairly consistent with historical data for angles up to 150° except for the species *C. autotrophica* (Fig. 10). It was highlighted in section 4 that depending on the algal species, VSF measurements can exhibit significantly different backscattering features beyond 150° (Fig. 4). Note that a strong variability in the far backward angles was also reported based on laboratory measurements of algae cultures [35]. Thus, our data corroborate the recent results obtained by Tan *et al*. [11] who advised to make use of at least two angular

#251344 Received 2 Oct 2015; revised 4 Dec 2015; accepted 4 Dec 2015; published 15 Dec 2015

measurements of the VSF, including one measurement at an angle larger than 150°, to minimize uncertainty sources especially in case of high concentration of hydrosols. This demonstrates the need of a better understanding of the directional effects of phytoplankton on light distribution within extremely turbid waters. Further research is also required to determine the shape of χ_p factors during a bloom of phytoplankton species occurring in a natural setting with all other co-occurring particles to verify if the results obtained here at laboratory could apply for realistic conditions.

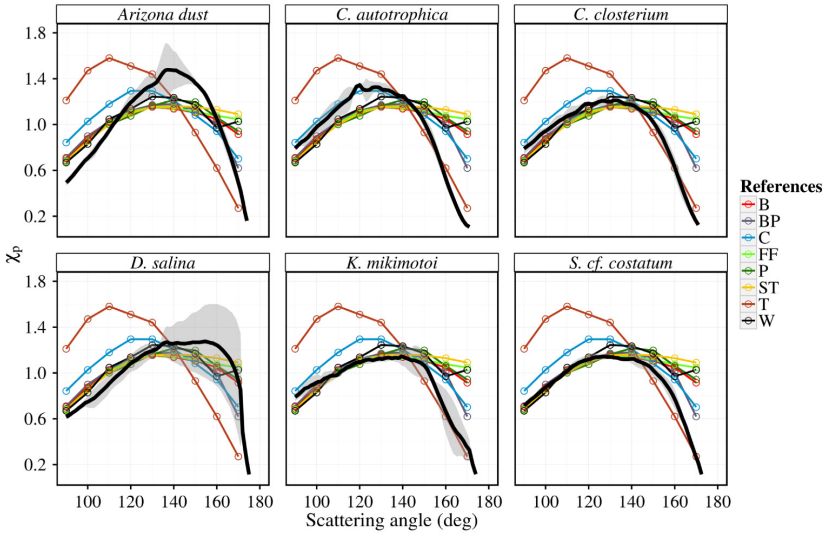

Fig. 10. Angular variation of χ_p factor from the combined I-VSF and POLVSM measurements (mean values, black line); the shaded area represents the two-standard-deviation interval. For comparison, χ_p factors taken from literature are shown: Berthon *et al.* [48] (B), Boss and Pegau [47] (BP), Chami *et al*. [49] (C), Fournier and Forand [38] (FF), Petzold [9] (P), Sullivan and Twardowski [15] (ST), Tan *et al.* [11] (T) and, Whitmire *et al*. [35] (W).

The χ_p factor of mineral-like hydrosols (i.e., Arizona dust) appears to be significantly different at angles greater than 130° from data found in the literature even though the best agreement with previous studies occurs for angles near 120°. Yet, a satisfactory retrieval of the backscattering coefficient of mineral-like hydrosols is of great interest due to the fact that dust aerosol depositions are frequent in certain regions of the world ocean. In particular, dust aerosol deposit events can dramatically change the underwater scattering properties and then potentially induce wrong interpretation of *in situ* or remote sensing data [50,51]. To explain the specific features observed at angles greater than 120°, Mie calculations were carried out using the measured size distribution of the Arizona dust sample (Fig. 2) for refractive indices values ranging from 1.14 to 1.18. Figure 11 shows the theoretical phase function and the χ_p factors together with the measurements. Although it was not possible to correctly match the measurements at angles lower than 120°, the simulations showed a good agreement with the data at large scattering angles (> 130°) for both the phase function (Fig. 11(a)) and the χ_p factor (Fig. 11(b)). Therefore, even if we are aware that the shape of the Arizona dust hydrosol may not be spherical, theoretical calculations confirm somehow that mineral-like hydrosols could have a significant increase of the phase function similar as what is measured here at angles larger than 120°. It is likely that the use of a correct particle size distribution (PSD) is important to satisfactorily reproduce the data. In natural waters, the PSD of the hydrosols may not commonly exhibit a size mode as large as the one measured during our experiment which could explain why our data differ from literature values for Arizona dust hydrosols. However, river runoffs or aerosol deposit for which particles are distributed around

#251344 Received 2 Oct 2015; revised 4 Dec 2015; accepted 4 Dec 2015; published 15 Dec 2015

a given size of mineral-like particles could potentially lead to angular variations of χ_p values similar as what we measured at angles greater than 120°.

Our data thus suggest to pay attention on the value of the χ_p factor that could be used for mineral-like particles dominated waters. At least, χ_p factor should not be derived using the measurement of the VSF performed at scattering angles greater than 130°, as it could be done for example by some commercially available backscattering sensors such as Hydroscat-Hobilabs instrument (i.e., the measurement of the VSF is made at 140°), to reduce the best as possible the error that could be made on b_{bp}.

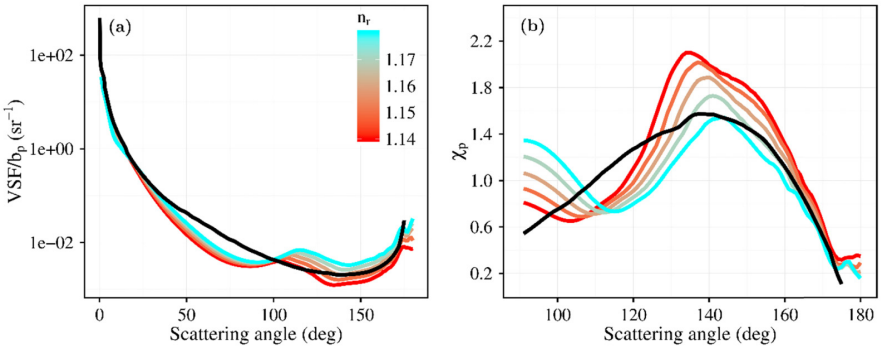

Fig. 11. Comparison of (a) the phase function and (b) the χ_p factor obtained from the Arizona dust measurements (black line) with Mie theory calculations (colored lines) performed for several refractive indices, n_r, from 1.14 to 1.18.

5. Conclusion

An original laboratory experiment was carried out to evaluate the accuracy of measuring the directional scattering properties of hydrosols in terms of volume scattering function. Measurements of five monospecific phytoplankton cultures and one mineral-like particle suspension were performed using three current VSF instruments, namely, I-VSF (HZG), LISST-VSF (Sequoia Scientific) and POLVSM (LOV). A rigorous protocol was used to ensure high quality cross-instrument measurements. In particular, special attention was paid to remove the effect of virus/bacteria within the biogenic samples to make sure the intrinsic phytoplankton cells scattering properties were measured. Following the protocol, the inter-comparison experiment was used (*i*) to provide the uncertainty attached to VSF measurements, and (*ii*) to analyze the angular shape of the VSF from 0.1 to 175° scattering angle. The mean relative standard deviations of the VSF measured by the instruments was around 10% for the mineral-like hydrosols and varied from 18% to 25% for phytoplankton. Such uncertainty values are acceptable given that VSF values vary by 6 orders of magnitude over the entire angular range. The uncertainty observed between the instruments was lowest for mineral-like hydrosols compared to algal samples, probably because of changes in phytoplankton cell size and structure during data acquisition. Relevant optical parameters such as the particulate scattering coefficient b_p and the backscattering ratio $\tilde{b}_{bp}$ (i.e., b_{bp}/b_p) were derived from the VSF data. The comparison of the b_p coefficient derived from VSF measurements with that derived using a combination of a transmissiometer and an integrating sphere (PSICAM) shows a strong agreement (R^2>0.98) with a dispersion of 0.1 m^{-1}, thereby confirming the good performance of the VSF meters instrument. The comparison of the backscattering ratio values $\tilde{b}_{bp}$ derived from the I-VSF and POLVSM instruments showed agreement within 3.5%.

The analysis of the phase function of the hydrosols (i.e., VSF / b_p) showed a significant increase of the measured VSF beyond the scattering angle value of 150° for all the phytoplankton species and for both the I-VSF and POLVSM instruments. Such angular

#251344 Received 2 Oct 2015; revised 4 Dec 2015; accepted 4 Dec 2015; published 15 Dec 2015

behavior was not observed for the widely used Fournier-Forand parameterization, despite the fact that a good agreement was observed between observations and FF approximations at angles lower than 150°. Our study thus suggests (*i*) to improve the theoretical modeling of hydrosols like phytoplankton internal structure and shape to better represent the increase of VSF at large scattering angles, (*ii*) to expand laboratory measurements of constituent-specific VSF, and (*iii*) to expand field measurements of *in situ* VSF to properly document the natural variability of the scattering by hydrosols at backward angles for remote sensing purposes. Further work in this direction will allow us to better retrieve the sole phytoplankton or mineral-like particles optical signature from the radiation measured by *in situ* or remote sensing devices. Finally, this study suggests that measuring the VSF at an angle larger than 150° in addition to the usual single measurement made at ~120° could likely improve the determination of particulate backscattering coefficient b_{bp} in natural waters.

6. Appendix

Phase functions (VSF/$b_{p,}$ in sr^{-1}) from 0.1° to 175° scattering angle (displayed in Fig. 9) are tabulated below for mineral-like hydrosol (Arizona dust 2 to 4.5 µm fraction) and phytoplankton species at the wavelength of 515 nm. Note that the phase functions tabulated here are the averaged values over the I-VSF, POLVSM and LISST-VSF instruments when the range of scattering angle overlaps between them.

Angles (deg)	Arizona dust	C. autotrophica	C. closterium	D. salina	*K. mikimotoi*	S. cf. costatum
0.10	4.21e + 02	-	2.55e + 02	3.23e + 02	7.85e + 02	7.38e + 02
0.15	2.80e + 02	-	2.55e + 02	3.13e + 02	8.55e + 02	6.50e + 02
0.20	1.39e + 02	-	2.70e + 02	3.59e + 02	8.54e + 02	5.26e + 02
0.30	7.80e + 01	-	2.40e + 02	2.98e + 02	7.44e + 02	4.16e + 02
0.40	5.73e + 01	3.18e + 01	2.24e + 02	2.82e + 02	6.19e + 02	3.17e + 02
0.50	4.79e + 01	3.12e + 01	2.08e + 02	2.56e + 02	4.79e + 02	2.59e + 02
0.75	3.98e + 01	3.02e + 01	1.51e + 02	2.04e + 02	2.15e + 02	1.62e + 02
1.00	3.34e + 01	2.82e + 01	1.11e + 02	1.52e + 02	7.70e + 01	1.07e + 02
1.25	3.17e + 01	2.78e + 01	8.31e + 01	1.14e + 02	4.13e + 01	8.14e + 01
1.50	2.96e + 01	2.69e + 01	6.19e + 01	7.74e + 01	3.11e + 01	6.29e + 01
2.00	2.57e + 01	2.46e + 01	4.29e + 01	2.87e + 01	2.01e + 01	4.01e + 01
2.50	2.23e + 01	2.23e + 01	3.15e + 01	9.65e + 00	1.37e + 01	2.78e + 01
3	1.36e + 01	1.80e + 01	1.67e + 01	9.62e + 00	7.73e + 00	1.47e + 01
4	9.20e + 00	1.31e + 01	9.97e + 00	6.07e + 00	5.19e + 00	8.28e + 00
5	6.22e + 00	9.03e + 00	5.73e + 00	3.35e + 00	3.75e + 00	4.67e + 00
7	3.17e + 00	4.13e + 00	2.74e + 00	1.40e + 00	2.27e + 00	2.38e + 00
9	1.98e + 00	2.34e + 00	1.53e + 00	7.76e-01	1.54e + 00	1.30e + 00
11	1.35e + 00	1.54e + 00	8.96e-01	4.90e-01	1.06e + 00	7.80e-01
13	9.69e-01	9.63e-01	5.57e-01	3.57e-01	7.59e-01	5.20e-01
15	7.11e-01	5.70e-01	3.58e-01	2.77e-01	5.56e-01	3.58e-01
17	4.75e-01	4.02e-01	2.25e-01	2.49e-01	3.70e-01	2.42e-01
19	3.60e-01	2.67e-01	1.61e-01	2.08e-01	2.73e-01	1.81e-01
21	2.79e-01	1.75e-01	1.15e-01	1.76e-01	2.00e-01	1.36e-01
23	2.24e-01	1.25e-01	8.67e-02	1.50e-01	1.45e-01	1.05e-01
25	1.79e-01	8.92e-02	6.60e-02	1.29e-01	1.05e-01	8.19e-02
27	1.44e-01	6.51e-02	5.06e-02	1.12e-01	7.76e-02	6.42e-02
29	1.18e-01	4.88e-02	3.97e-02	9.73e-02	5.82e-02	5.10e-02
31	9.77e-02	3.72e-02	3.18e-02	8.52e-02	4.51e-02	4.09e-02
33	8.18e-02	2.87e-02	2.56e-02	7.61e-02	3.64e-02	3.30e-02
35	6.93e-02	2.28e-02	2.07e-02	6.78e-02	3.02e-02	2.66e-02
37	5.95e-02	1.84e-02	1.72e-02	6.04e-02	2.59e-02	2.20e-02
39	5.17e-02	1.50e-02	1.44e-02	5.38e-02	2.24e-02	1.82e-02
41	4.54e-02	1.25e-02	1.21e-02	4.82e-02	2.00e-02	1.53e-02
43	3.99e-02	1.05e-02	1.03e-02	4.36e-02	1.76e-02	1.28e-02
45	3.55e-02	8.88e-03	8.82e-03	3.92e-02	1.56e-02	1.08e-02
47	3.16e-02	7.60e-03	7.67e-03	3.57e-02	1.38e-02	9.18e-03
49	2.82e-02	6.55e-03	6.59e-03	3.24e-02	1.19e-02	7.97e-03
51	2.53e-02	5.65e-03	5.67e-03	2.94e-02	1.03e-02	6.89e-03
53	2.27e-02	4.95e-03	4.92e-03	2.70e-02	8.89e-03	5.99e-03

#251344 Received 2 Oct 2015; revised 4 Dec 2015; accepted 4 Dec 2015; published 15 Dec 2015

55	2.04e-02	4.34e-03	4.27e-03	2.49e-02	7.69e-03	5.26e-03
57	1.84e-02	3.81e-03	3.70e-03	2.31e-02	6.67e-03	4.69e-03
59	1.64e-02	3.37e-03	3.20e-03	2.15e-02	5.92e-03	4.20e-03
61	1.48e-02	3.00e-03	2.83e-03	2.01e-02	5.37e-03	3.78e-03
63	1.34e-02	2.68e-03	2.50e-03	1.88e-02	4.90e-03	3.42e-03
65	1.21e-02	2.40e-03	2.24e-03	1.76e-02	4.49e-03	3.13e-03
67	1.09e-02	2.16e-03	2.02e-03	1.64e-02	4.20e-03	2.87e-03
69	9.83e-03	1.95e-03	1.85e-03	1.55e-02	3.91e-03	2.64e-03
71	8.86e-03	1.77e-03	1.71e-03	1.45e-02	3.60e-03	2.45e-03
73	8.02e-03	1.62e-03	1.58e-03	1.36e-02	3.37e-03	2.28e-03
75	7.27e-03	1.48e-03	1.47e-03	1.29e-02	3.12e-03	2.12e-03
77	6.62e-03	1.36e-03	1.38e-03	1.22e-02	2.91e-03	1.99e-03
79	6.01e-03	1.26e-03	1.30e-03	1.15e-02	2.72e-03	1.87e-03
81	5.48e-03	1.17e-03	1.22e-03	1.09e-02	2.54e-03	1.75e-03
83	5.01e-03	1.10e-03	1.15e-03	1.03e-02	2.37e-03	1.66e-03
85	4.60e-03	1.03e-03	1.10e-03	9.73e-03	2.22e-03	1.57e-03
87	4.22e-03	9.77e-04	1.05e-03	9.24e-03	2.11e-03	1.49e-03
89	3.90e-03	9.22e-04	1.01e-03	8.77e-03	2.00e-03	1.42e-03
91	3.61e-03	8.75e-04	9.67e-04	8.35e-03	1.92e-03	1.35e-03
93	3.35e-03	8.29e-04	9.37e-04	7.90e-03	1.84e-03	1.29e-03
95	3.11e-03	7.96e-04	8.99e-04	7.55e-03	1.75e-03	1.24e-03
97	2.89e-03	7.59e-04	8.62e-04	7.19e-03	1.71e-03	1.18e-03
99	2.71e-03	7.31e-04	8.41e-04	6.85e-03	1.67e-03	1.14e-03
101	2.55e-03	7.01e-04	8.23e-04	6.56e-03	1.65e-03	1.10e-03
103	2.40e-03	6.73e-04	7.91e-04	6.30e-03	1.62e-03	1.07e-03
105	2.26e-03	6.50e-04	7.64e-04	6.02e-03	1.59e-03	1.03e-03
107	2.15e-03	6.27e-04	7.51e-04	5.80e-03	1.58e-03	1.00e-03
109	2.05e-03	6.12e-04	7.34e-04	5.58e-03	1.59e-03	9.71e-04
111	1.95e-03	5.92e-04	7.14e-04	5.38e-03	1.53e-03	9.50e-04
113	1.87e-03	5.73e-04	7.05e-04	5.18e-03	1.51e-03	9.30e-04
115	1.80e-03	5.61e-04	6.98e-04	5.01e-03	1.48e-03	9.09e-04
117	1.73e-03	5.53e-04	6.81e-04	4.85e-03	1.45e-03	8.97e-04
119	1.67e-03	5.42e-04	6.71e-04	4.71e-03	1.43e-03	8.88e-04
121	1.63e-03	5.39e-04	6.73e-04	4.57e-03	1.42e-03	8.81e-04
123	1.58e-03	5.30e-04	6.67e-04	4.46e-03	1.39e-03	8.68e-04
125	1.54e-03	5.34e-04	6.54e-04	4.35e-03	1.39e-03	8.62e-04
127	1.51e-03	5.32e-04	6.50e-04	4.28e-03	1.40e-03	8.59e-04
129	1.48e-03	5.33e-04	6.61e-04	4.26e-03	1.38e-03	8.58e-04
131	1.46e-03	5.39e-04	6.58e-04	4.24e-03	1.39e-03	8.50e-04
133	1.44e-03	5.43e-04	6.53e-04	4.26e-03	1.37e-03	8.53e-04
135	1.42e-03	5.52e-04	6.60e-04	4.32e-03	1.39e-03	8.55e-04
137	1.41e-03	5.66e-04	6.68e-04	4.37e-03	1.37e-03	8.54e-04
139	1.38e-03	5.77e-04	6.64e-04	4.44e-03	1.34e-03	8.51e-04
141	1.37e-03	5.85e-04	6.72e-04	4.47e-03	1.34e-03	8.40e-04
143	1.37e-03	6.06e-04	6.91e-04	4.53e-03	1.34e-03	8.54e-04
145	1.37e-03	6.26e-04	7.08e-04	4.55e-03	1.34e-03	8.65e-04
147	1.38e-03	6.55e-04	7.29e-04	4.59e-03	1.34e-03	8.79e-04
149	1.39e-03	7.00e-04	7.74e-04	4.62e-03	1.37e-03	9.00e-04
151	1.43e-03	7.60e-04	8.24e-04	4.65e-03	1.44e-03	9.38e-04
153	1.46e-03	8.39e-04	8.94e-04	4.70e-03	1.59e-03	9.75e-04
155	1.51e-03	9.43e-04	9.81e-04	4.73e-03	1.84e-03	1.01e-03
157	1.59e-03	1.09e-03	1.10e-03	4.82e-03	2.16e-03	1.06e-03
159	1.70e-03	1.31e-03	1.25e-03	4.91e-03	2.57e-03	1.13e-03
161	1.83e-03	1.63e-03	1.53e-03	5.05e-03	3.10e-03	1.26e-03
163	2.01e-03	2.07e-03	1.93e-03	5.30e-03	3.76e-03	1.47e-03
165	2.25e-03	2.78e-03	2.46e-03	5.63e-03	4.28e-03	1.74e-03
167	2.61e-03	4.09e-03	3.32e-03	6.14e-03	4.51e-03	2.31e-03
169	3.18e-03	5.88e-03	4.70e-03	7.04e-03	5.14e-03	3.27e-03
171	4.37e-03	8.87e-03	7.48e-03	8.93e-03	5.71e-03	5.23e-03
173	7.92e-03	1.91e-02	1.54e-02	1.50e-02	9.70e-03	1.05e-02
175	2.00e-02	5.08e-02	4.60e-02	4.57e-02	3.69e-02	3.10e-02

#251344 Received 2 Oct 2015; revised 4 Dec 2015; accepted 4 Dec 2015; published 15 Dec 2015

Acknowledgments

The authors are grateful to the following institutions for their financial support: French space agency CNES, Institut Universitaire de France, Université Pierre et Marie Curie, Helmholtz-Zentrum Geesthacht, and Sequoia Inc. The authors would like to thank all the staff that helped for performing some of the measurements presented in this study: Sophie Marro (*Laboratoire d'Océanographie de Villefranche*-LOV), Amélie Talec (LOV), Typhaine Lecieux (LOV), Charlotte Combes (LOV), Wolfgang Schönfeld (HZG), and the culture service of Roscoff (*Université Pierre et Marie Curie*, France). We also would like to thank Yogi Agrawal (Sequoia), Deric Gray (U.S. Naval Research Lab), and David McKee (University of Strathclyde, UK), which were unfortunately not able to attend to the experiment, for helpful discussions when preparing the inter-comparison experiment. The authors are grateful to the anonymous reviewers for their relevant comments and suggestions.

#251344 Received 2 Oct 2015; revised 4 Dec 2015; accepted 4 Dec 2015; published 15 Dec 2015